Journal of Agriculture and Food Research 6 (2021) 100251

Contents lists available at ScienceDirect

Journal of Agriculture and Food Research

journal homepage: www.sciencedirect.com/journal/journal-of-agriculture-and-food-research

Feasibility of utilizing color imaging and machine learning for adulteration detection in minced meat

Ahmed M. Rady [a,c], Akinbode Adedeji, Ph.D. [b,*], Nicholas J. Watson [a]

[a] Food, Water, Waste Research Group, Faculty of Engineering, University of Nottingham, University Park, Nottingham, NG7 2RD, UK
[b] Department of Biosystems and Agricultural Engineering, University of Kentucky, Lexington, USA
[c] Teagasc Food Research Centre, Ashtown, Dublin, Ireland

ARTICLE INFO

Keywords:
Machine learning
RGB
Meat adulteration
Industry 4.0
Digital manufacturing
Non-invasive sensing

ABSTRACT

Meat products are popular foods and there is a need for cost-effective technologies for rapid quality assessment. In this study, RGB color imaging coupled with machine learning algorithms were investigated to detect plant and animal adulterants with ratios of from 1 to 50% in minced meat. First, samples were classified as either pure or adulterated, then adulterated samples were classified based on the adulterant's type. Finally, regression models were developed to predict the adulteration quantity. Linear discriminant classifier enhanced by bagging ensembling performed the best with overall classification accuracies for detecting pure or adulterated samples up to 99.1% using all features, and 100% using selected features. Classification accuracies for adulteration origin were 48.9–76.1% using all features and 63.8% for selected features. Regression trees were used for adulterant level quantification and the r (RPD) values were up to 98.0%(5.0) based on all features, and 94.5%(3.2) for selected features. Gray-level and co-occurrence features were more effective than other color channels in building classification and regression models. This study presents a non-invasive, and low-cost system for adulteration detection in minced meats.

1. Introduction

In 2017, the total world production of cattle, pigs, and chickens reached 295,193 million Metric Tonnes, making meat the largest produced agricultural product by volume [1]. Meat and poultry processing is the largest sector in the US food industry, with a $1020 billion contribution to the economy in 2016, providing over 5.4 million jobs [2]. Food fraud is the deliberate act of substituting, adding, tampering, or misrepresentation of food, food ingredients, or food packaging [3]. Therefore, preventing food fraud is essential for food manufacturers, retailers, fast food chains, and consumers. The meat industry has seen a significant surge of food fraud in 2013 when the "horsemeat scandal" was discovered in Ireland, England, and Luxemburg. Minced beef burgers were adulterated with up to 100% minced horsemeat and/or pork which opposes some ethical and religious groups [4]. This incident damaged the reputation of meat producers and retailers in the UK and Ireland and further highlighted the need for rapid and cost-effective techniques that can identify adulterants in minced meats in early processing stages.

A fresh beef muscle contains water (~72%), protein (~21%), lipid (~5%), carbohydrate (~1%), and ash (~1%) [5]. Major processed meat products include minced beef, hamburgers, beef patties, cooked ham, cooked sausages, bacon, canned products, dry-cured ham, mold-ripened sausages, semi-dry, and dry fermented sausages [6,7]. For beef patties or burgers, several ingredients are added to the minced beef during processing to enhance flavor and fat emulsification, to ensure a consistent shape by increasing the water-binding properties, and to act as fillers for cost reduction These ingredients include water, salt, soy proteins wheat gluten, and milk proteins [8]. Functional ingredients such as isolated soy protein or non-fat dried milk proteins are usually added at approximately 2%. Meat extenders and fillers such as soy flour, soy concentrate, beans, peas, lentils, cereal flours, starches are added at around 15% [7]. Consequently, the likelihood of adulterating a processed meat product will mostly be achieved by adding an excess of fillers such as wheat gluten, or soy proteins as they are cheaper than meat.

The common laboratory-based techniques for identifying foreign or unwanted proteins in processed beef are electrophoresis, immunological reactions, and chromatography [9]. Examples of these techniques include detecting soybean and milk proteins in sterilized beef patties using SDS-PAGE [10], using ELISA to estimate soybean, and pea

* Corresponding author.
E-mail addresses: ahmed.rady1@nottingham.ac.uk (A.M. Rady), akinbode.adedeji@uky.edu (A. Adedeji), nicholas.watson@nottingham.ac.uk (N.J. Watson).

https://doi.org/10.1016/j.jafr.2021.100251
Received 1 August 2021; Received in revised form 27 November 2021; Accepted 3 December 2021
Available online 5 December 2021
2666-1543/© 2021 The Authors. Published by Elsevier B.V. This is an open access article under the CC BY-NC-ND license (http://creativecommons.org/licenses/by-nc-nd/4.0/).

proteins, and wheat gluten in sausages [11], utilizing Ion-exchange HPLC for tracking soybean proteins, caseins, and whey proteins in processed meats [12], and using PCR test to detect the characterizing DNA of animal-based adulterants in meat samples [13]. Although the previous methods have shown high accuracy and resolution in identifying various types of foreign proteins in processed meats, they still have several drawbacks including, relatively long sampling time, high cost, and the requirement of highly skilled workers. Therefore, such methods are not suitable for rapid, and online authentication within the meat supply chain.

The applications of optical sensors for the evaluation of meat quality and safety has been extensively studied. Detection of horsemeat in minced beef was studied using visible(Vis)/near-infrared (NIR) spectroscopy, and Vis/NIR hyperspectral imaging (400–1000 nm) with a maximum R^2 value of 98% for regression models [14]. Distinguishing pork in minced beef using Vis/NIR multispectral imaging was feasible with 98% overall classification accuracy [15]. Al-Sarayreh, M Reis [16] studied the application of Vis/NIR hyperspectral imaging (548–1701 nm) to identify beef or pork in lamb meat and achieved a classification accuracy of 94.4%. Other studies include utilizing spectroscopic systems to assess minced beef adulterated with turkey meat [17], using Vis/NIR spectroscopy (400–2500 nm) to detect pork, fat trimming, and offal in fresh and frozen-thawed minced beef [18], and assessing minced beef and pork adulterated with soybean and wheat gluten by Vis/NIR spectroscopic [19] and hyperspectral imaging systems [20].

Color Vision (CV) is a tri-waveband imaging technique that acquires spectral information about an object on the Red, Green, Blue (RGB) color channels. CV has been used to perceive external defects in fruits and vegetables and is significantly lower in cost compared with other optical systems [21,22]. The utilization of CV in meat quality comprised identifying quality parameters of beef such as color [23–25], marbling [25–27], intramuscular fat [28], lean meat content [29], and palatability [30]. CV was also used for pork quality such as assessing color [31–36], freshness [37], and intramuscular fat content [38]. Other applications were about quality tracking of chicken and lamb [39]. CV systems were studied for detecting fraudulent frozen bovine meat where images of histological cuts of bovine were classified against those injected with water-based solutions, and a Support Vector Machine (SVM) classifier showed a classification accuracy of 96.6% [40]. However, the application of CV systems for detecting adulteration in beef or pork has not been studied before. Therefore, the objective of this study is to assess the feasibility of using a low-cost CV system and machine learning methods to detect plant and animal protein adulterants in minced beef and pork meats. In this study, models were developed to detect if a sample contains adulterants before determining the origin and quantity of the adulterant. The study also explored the effect of different featured engineering methods on the performance of the machine learning models.

2. Materials and methods

2.1. Materials and experimental design

The meat samples utilized in this study were beef (chuck roast), pork (Boston Butt), and chicken thigh. Additionally, textured soybean protein (SP) (Red Mill, Milwaukie, Oregon, USA), which is a soy flour containing 50% protein, and wheat gluten (WG) (TruTex RS 65, MGP, Atchison, Kansas, USA), which includes 75% protein were used as adulterants. The SP or WG had relatively larger particles as shown in Fig. 1compared with those are commonly used in beef patty processing. However, the referred plant proteins were chosen to study the feasibility of applying the RGB color sensor for evaluating beef or pork adulteration. Meat samples were bought from a local store in Lexington, State of Kentucky, USA. The sources of the meat were farms in the State of Kentucky. Meat samples were stored at 1 °C until they were minced and imaged. The grinding process took place using a kitchen grinder (Kitchen Aid, Benton Harbor, Michigan, USA) at an approximate speed of 60 rpm. Grinder parts were carefully washed between each consecutive grindings with warm water and soap, then dried using paper towels. SP was prepared by stirring dry SP with boiling water at 100 °C (1:2.6, w:w) in a stainless steel bowl for 10 min. It was then added to the meat at the required quantity. WG was prepared by stirring dry WG with warm water at approximately 50 °C (1:3.5, w:w) in a stainless steel pan for 20 min until the water was completely absorbed. It was then added to the meat at the required quantity. The surface of each sample was flattened using a round glass disc to minimize the impact of surface topography on the recorded images and subsequent analysis.

The prepared samples were pure meat (i.e., beef, pork, chicken, SP, and WG) and adulterated samples (Beef + Pork, Beef + SP, Beef + Chicken, Beef + WG, Pork + SP, and Beef + Pork + SP). For each mixture, the first material is the adulterated and the rest is the adulterant (s). There were 14 ratios of adulteration of pork in beef with a range of 1–50% (w/w), while 21 different ratios of SP, chicken, and WG were used to adulterate the beef with ranges between 1 and 40%. The pork was adulterated with SP (21 ratios, 1–40%). Finally, beef samples were adulterated simultaneously with pork and SP, the ratios of pork and SP adulteration in beef varied such that the pork portions were 50, 40, 33.3, 25, and 20%, whereas the equivalent SP portions were 33.3, 40, 25, 50, and 60% [19]. Adulterated samples were prepared by manually mixing the desired components for 10–20 s until complete mixing was achieved. Approximately 30 ± 5 g of each sample was weighed, shaped into a uniform disc, flattened and then placed in a petri dish and flatten until imaged. Each sample was prepared individually and the manual mixing was chosen over a specialized mixer to minimize sample preparation time (e.g. equipment cleaning) which may induce changes (e.g. color) in the samples. Fig. 1 displays the color images of the tested samples (pure and adulterated) along with the number of samples that were imaged. The total number of adulterated samples was 1545 compared with 152 pure samples which is due to the range of different adulterants and adulterants' ratios investigated in this study.

2.2. Color vision (CV) system

A schematic configuration of the CV system utilized in this study is shown in Fig. 2. The system contained a Fiber-Lite illuminator (MI-150, Dolan-Jenner, Boxborough, MA, USA) with a halogen lamp (output power of 150 W) and two light guides (EEG 2823 M, Dolan-Jenner, Boxborough, MA, USA). These were horizontally inclined at an angle of 57° and located 26 cm vertically above the samples. A CMOS (complementary metal-oxide semiconductor) color digital camera (Coolpix P520, Nikon Corporation, Minato, Tokyo, Japan) was used to acquire the images. The imaging configurations were determined via preliminary trials and included mounting the camera 23 cm above the surface of the samples and setting the angle between the camera lens axis and the light beam to be around 33°. To ensure a consistent illumination condition, the camera along with the lighting guides were enclosed in a black wooden box. The petri dish containing the sample was placed on a black surface. Each image was captured with no flash, and the output image was saved in JPEG format with 3672x4896 pixels.

2.3. Image processing

2.3.1. Segmentation of the region of interest

RGB (red, green, and blue) and HSI (hue, saturation, and intensity) color coordinates are common in color image analysis, with the latter system being more representative of human vision [41]. While RGB illustrates each color channel in its spectral region, hue, saturation, and intensity describe a pure color, the dilution degree of a pure color by white light, and the brightness of the object, respectively [42]. Each RGB image was transformed into the HSI space. The data used in subsequent feature extraction included the red, green, blue channels, gray-level images, in addition to the saturation component of the HSI color

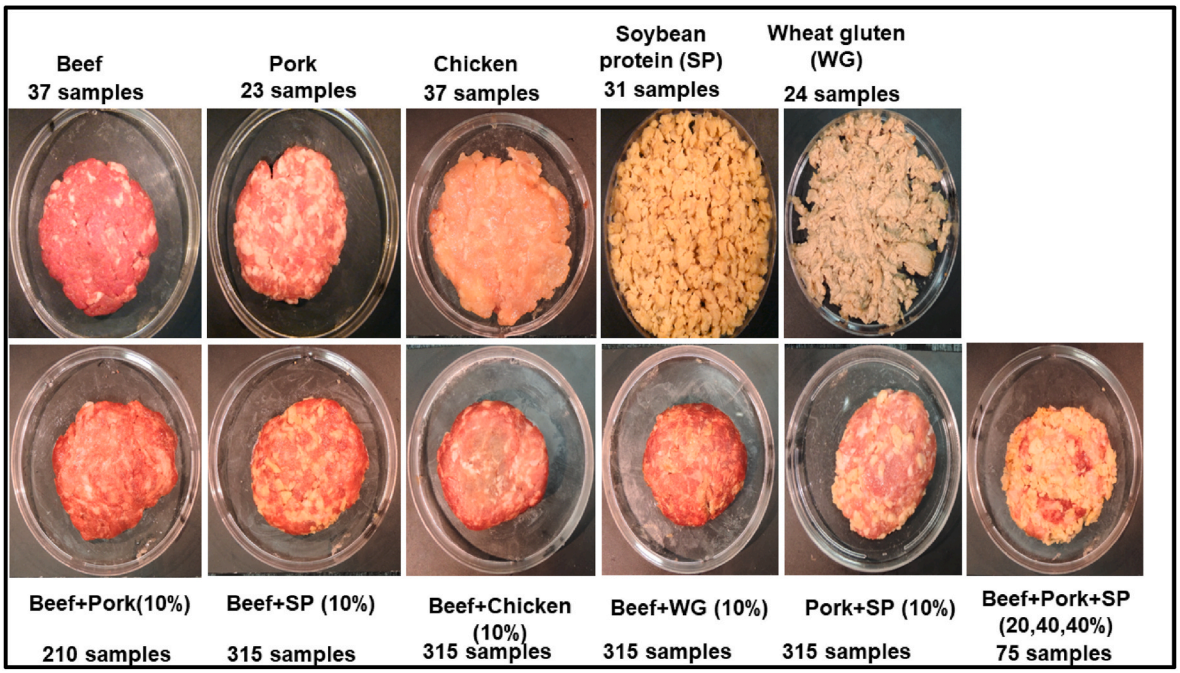

Fig. 1. Examples of color images of the pure and adulterated meat samples utilized in this study. The mixtures are stated as adulterated + adulterant. The number in parenthesis refers to the adulteration level for the referred adulterant. (For interpretation of the references to color in this figure legend, the reader is referred to the Web version of this article.)

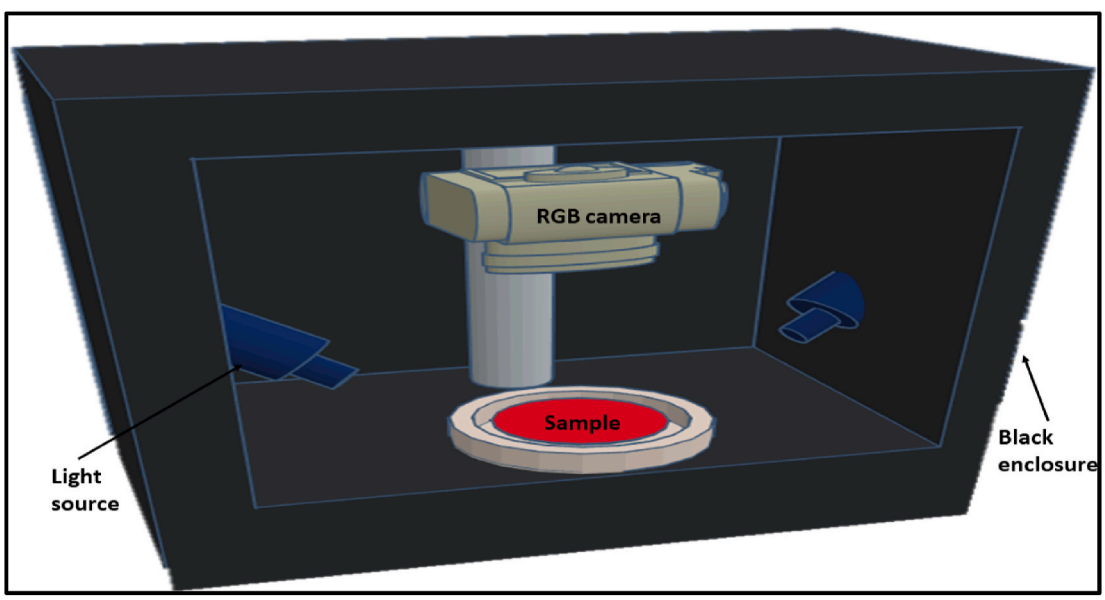

Fig. 2. Schematic diagram of the RGB vision system used to acquire color images for pure and adulterated meat samples. (For interpretation of the references to color in this figure legend, the reader is referred to the Web version of this article.)

space. The saturation coordinate represents how much the studied color value is diluted with the white light [43].

To obtain the Region of Interest (ROI), color segmentation using k-means clustering was applied, based on the International Commission on Illumination (CIE) L*a*b* color space where L*, a*, and b* refer to lightness from black to white, green to red component, and blue-yellow component, respectively [41,44]. The objects in each image were the sample ROI, the petri dish, and the background. First, the image was converted into the L*a*b*, and only the a*b* coordinates were considered as they hold the color information. K-means clustering was then applied assuming the k value to be 3 (i.e., no. of objects in each image). The binary mask image was then obtained by choosing the clustered image containing the ROI and projecting it on the original RGB image before applying dilation. The ROI segmented color and gray-level images were finally calculated by applying the binary mask on the original RGB image. A transform was applied to generate a gray-level image. Fig. 3 displays the segmentation process utilized in this study.

2.3.2. Feature extraction

Based on preliminary analysis, the image features required for the machine learning models were extracted from the red (R), green (G), and blue (B) channels in the RGB color space, and the saturation (S)

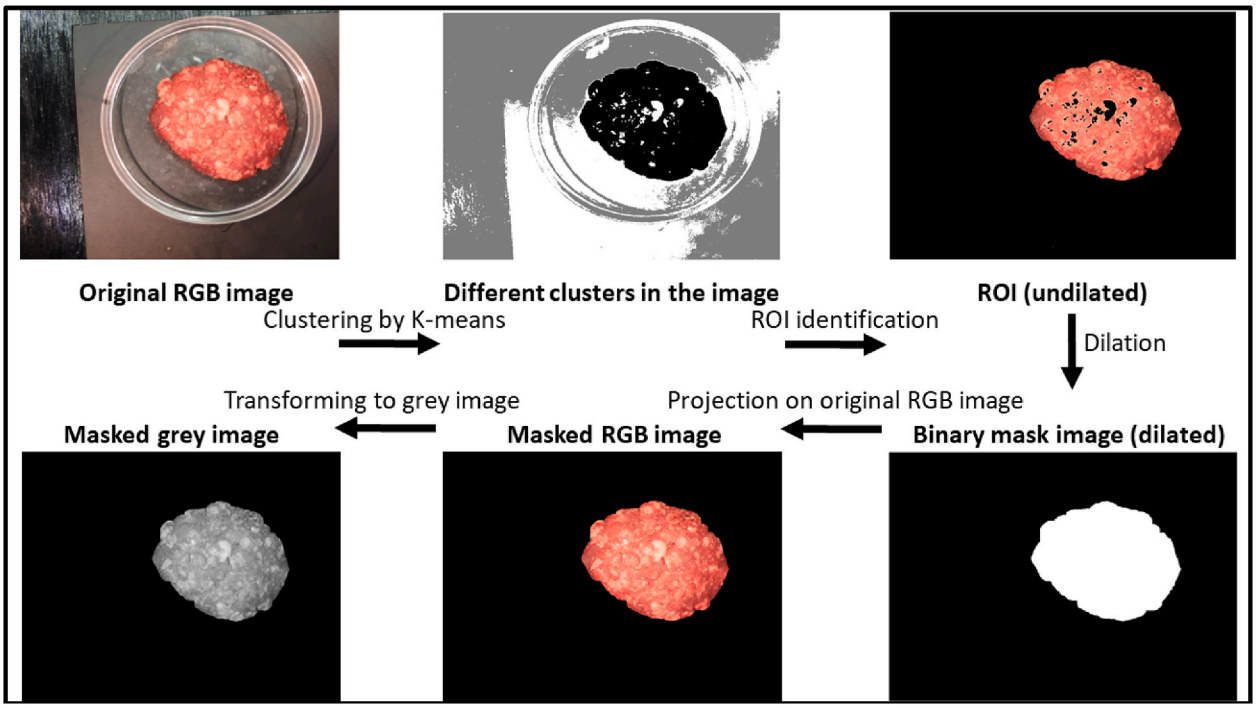

Fig. 3. Summary of segmentation steps followed to obtain the region of interest (ROI) from the initial RGB image.

coordinate in the HSI color space. Additionally, the gray-level images were used in the data analysis. The aim of studying so many features was to investigate the effect that different image features have on machine learning model performance. Features extracted from gray-level images are commonly used in color imaging analysis, which is why they were studied in this work [45].

2.3.2.1. Histogram-based features. One of the simplest methods that can be used for image description is the histogram-based features or first-order statistics that calculate different parameters for describing objects in an image [41]. The calculated features were mean, variance, and third moment of the ROI histogram (3 features). z represent the intensity level in an image for any of the aforementioned four-color coordinates in the range of [0,L-1], $p(z_i)$ represents the normalized histogram component corresponding to the *ith* r value and can be considered as an estimate of the probability of the occurrence of the intensity level r_i, and L as the number of possible intensity levels. The mean (m), variance (s), and 3rd moment (μ_3 (z)) can then be calculated as follows:

$$m = \sum_{i=0}^{L-1} z_i \, p(z_i)$$

$$s = \sum_{i=0}^{L-1} (z_i - m)^2 p(z_i)$$

$$\mu_n = \sum_{i=0}^{L-1} (z_i - m)^3 p(z_i)$$

2.3.2.2. Spectral measures of texture. Spectral measures of texture uses the Fourier spectrum to represent distinguishing periodic and non-periodic patterns in images [46]. These features are extracted in polar coordinates (r, θ) and include S(r), and S(θ). S(r) represents the spectrum at all r values and a fixed θ value, whereas the S(θ) represents the spectrum at all θ values and a fixed r value. Each function can be calculated as follows:

$$s(r) = \sum_{\theta=0}^{\pi} S_\theta(r)$$

$$s(\theta) = \sum_{\theta=0}^{\pi} S_r(\theta)$$

Where $S_r(\theta)$ and $S_\theta(r)$ are a one-dimensional function in θ and r, respectively. In this study, the θ varies from 0-π (180 values) and is normalized between [0–1]. Only the maximum value was considered for the S(r), and the first 10 values were considered for S(θ). Thus, the total number of spectral features was 11.

2.3.2.3. Texture features derived from the co-occurrence matrix. Texture features calculated based on the co-occurrence matrix considers the intensity distribution as well as the spatial position of two neighbor pixels in an image [41]. Thus, COM is a common measure of image texture. Texture features extracted in this study were adapted from the work by Haralick, Shanmugam [47] and included contrast, correlation, sum of squares or variance, inverse difference moment, sum average, sum variance, sum entropy, difference, difference variance, entropy, information measures of correlation 1, information measures of correlation 2 and the inverse difference moment. Assuming that P is the normalized form of the gray-level co-occurrence matrix (GLCM) of an image I, p(i,j) is the (*i,j*)th entry in P, x and y represent the spatial coordinates of P. P_x and P_y are the *ith* and *jth* entries in the matrices obtained by summing the rows and columns of P, respectively. μ_x, μ_y, σ_x, σ_y are the means and standard deviations of P_x and P_y, μ is the mean value of P, and N_g is the number of gray-level images used. Therefore, the following equations can be developed based on the work by Haralick et al. (1973):

$$Correlation = \frac{\sum_i \sum_j (ij) p(i,j) - (\mu_x \mu_y)}{\sigma_x \sigma_y}$$

$$Contrast = \sum_{n=0}^{N_g - 1} n^2 \left\{ \sum_{i=1}^{N_g} \sum_{J=1}^{N_g} p(i,j) \right\}_{|i-j|=n}$$

$$Sum\ of\ squares, variance = \sum_i \sum_j (i-\mu)^2\, p(i,j)$$

$$Inverse\ difference\ moment = \sum_i \sum_j \frac{1}{1+(i-j)^2}\, p(i,j)$$

$$Sum\ average = \sum_{i=2}^{2N_g} iP_{x+y}(i)$$

$$\text{Where } P_{x+y}(k) = \{\sum_{i=1}^{N_g}\sum_{J=1}^{N_g} p(i,j)\}_{i+j=k,\ k=2,\ 3,\ \ldots,\ 2N_g}$$

$$Sum\ entropy = SE = -\sum_{i=2}^{2N_g} P_{x+y}(i) log\{P_{x+y}(i)\}$$

$$Sum\ variance = \sum_{i=2}^{2N_g} (i-SE)^2 P_{x+y}(i)$$

$$Entropy = -\sum_i \sum_j p(i,j)\log(p(i,j))$$

$$Difference\ variance = variance\ of\ p_{x-y}$$

$$Difference\ entropy = -\sum_{i=0}^{N_g-1} P_{x-y}(i) log\{P_{x-y}(i)\}$$

$$\text{Where. } P_{x-y}(k) = \{\sum_{i=1}^{N_g}\sum_{J=1}^{N_g} p(i,j)\}_{i-j=k}$$

Texture features commonly used by other researchers were also calculated incorporating homogeneity, uniformity, and maximum probability [41], cluster prominence and cluster shade [48], autocorrelation [42], dissimilarity [49], and inverse difference [50]. The total texture features extracted were 20.

2.3.2.4. Principal component features. Principal Component Analysis (PCA) has several applications in multivariate analysis including dimension reduction, transforming highly correlated data to uncorrelated variables, and data visualization [51]. Principal components can be used for describing sets of images registered spatially with different intensities for pixels having the same location, such as the three channels in an RGB image [41]. In this study, only 5 eigenvalues were considered, and these represented ≥99% of the total variance.

2.3.2.5. Invariant moments. Invariant moments are 2-D moments derived from the normalized central moments with different orders [41]. Invariant moments are not affected by translation, scale change, mirroring, or rotation. In this study, 7 invariant moments were calculated. Table 1 summarizes the extracted features from the RGB images. For each color coordinate, 46 features were calculated.

2.4. Data analysis

2.4.1. Feature engineering

The different features calculated for each image were concatenated and normalized before developing the machine learning models. Based on the number of samples in this study, there were 108 classes comprising 5 pure samples and 103 adulterated samples, corresponding to different types and ratios of adulteration Given this number of class, conducting a one-step classification would require a much larger data set. Therefore, it was decided to perform the analysis in three consecutive stages with different classification and regression models for each stage. In the first stage, a binary classification model was developed to classify each sample into pure (i.e. unadulterated) (1 class) or adulterated (1 class). The second stage was to determine the adulterant type. Therefore, only the data for adulterated samples was used in the second stage. The second stage models were trained based on 6 output classes (Beef + Pork, Beef + SP, Beef + Chicken, Beef + WG, Pork + SP, or Beef + Pork + SP). The third stage aimed to quantify the level of adulteration by developing regression models. The complete flow of the analysis followed in this study is shown in Fig. 4. To overcome the problem of an imbalanced dataset in the first stage where there are 152 pure samples vs. 1545 adulterated samples, resampling using downsampling, and oversampling was applied [52]. Downsampling was conducted such that the adulterated class was reduced to 154 samples, that included approximately 26 samples in each adulterated sub-class, and 9 different possibilities of the adulterated class depending on the selected samples. For the oversampling scheme, two techniques were utilized, the pure class was either resampled to reach 1520 samples, or the Synthetic Minority Over-sampling Technique (SMOTE) was applied [52–54].

Although the several types of features implemented in this study, it was worth studying the most effective variables for classification or quantification. Feature selection was addressed using sequential feature selection either for classification based on DT or for regression based on RT.

Table 1
Extracted features from each color coordinate.

Type of features	Extracted features
Histogram-based features	3
Spectral measures of texture	11
GLCM texture features	20
Principal component features	5
Invariant moments	7
Total no. of features for each color coordinate	46

2.4.2. Development of classification models

To develop classification models, Linear Discriminant Analysis (LDA) boosted by the ensemble methodology to enhance the classifier's performance. The LDA classifier is simple to implement and relatively fast to train compared with artificial neural networks [55]. The classifier includes a linear combination of the features and is based on the value of the discriminant function before the sample (i.e., image) is classified into the appropriate class [56]. Ensemble techniques are based on optimizing the classification performance by weighing several individual classifiers and combining them to obtain a classifier that out-performs the single classifier [57]. Among several ensemble methods, the bagging technique was applied in this study. The purpose of ensemble bagging is to form a better-performing classifier from a number of weaker performing classifiers, where each weak classifier is a result of training the samples with replacement [57]. The number of weak classifiers used in this study was 10. The data were divided into training (80%) and testing (20%) sets and cross-validation (10-fold) was applied to the training set to obtain the best model. This model was then applied on the separate test set, and the classification accuracy was reported.

2.4.3. Development of regression models

To develop regression models for determining the quantity of adulterant in each adulterated sample, Regression Trees (RT) models were developed. Classification and regression trees are based on sequential partitioning of the input feature space into several binary sub-regions based on model parameters. The sample is then classified into the class that has the minimum error [58]. In the RT algorithm, the input features are partitioned into regions, and a regression model is fitted based on the features in each region with the objective to find the optimal partitioning variables and points [51]. Samples were divided into calibration (80%) and validation (20%) sets. Cross-validation (10-fold) was then implemented on the calibration set, and the best validation model was reported based on the correlation coefficient (r), Root Mean Square Error of Cross-Validation ($RMSE_{CV}$), and the Residual

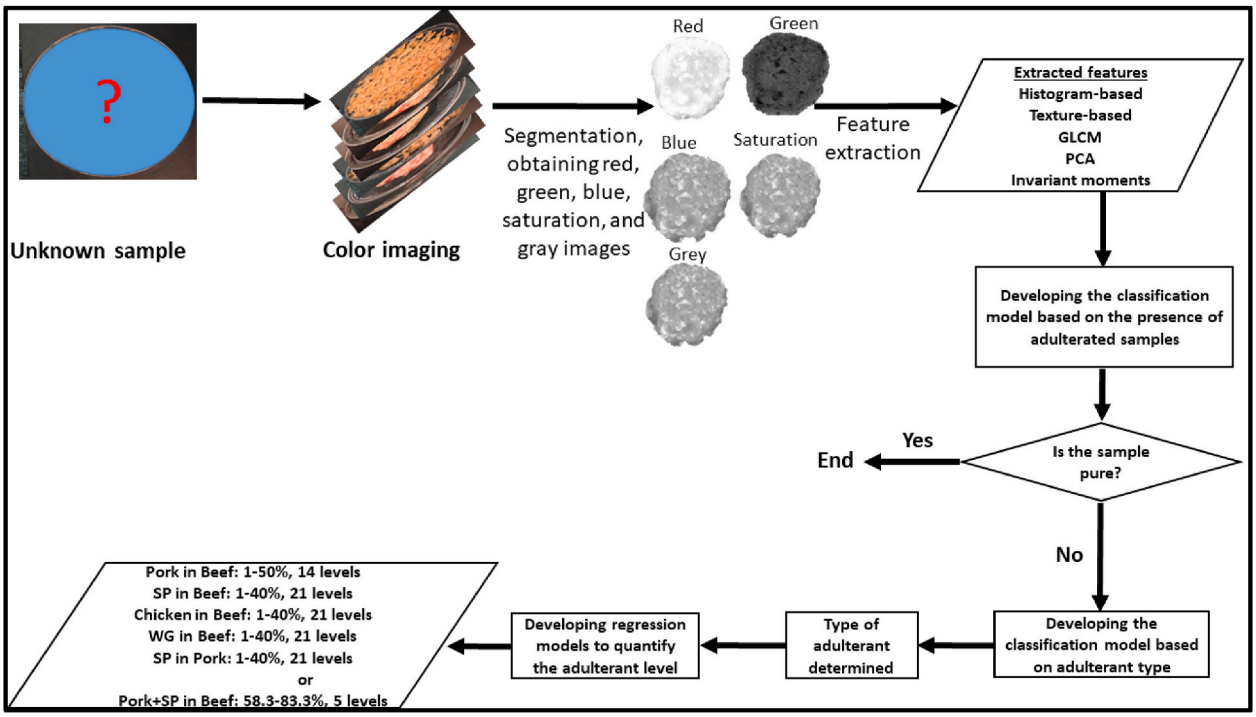

Fig. 4. Data analysis steps followed during the study to determine and quantify the adulterant in minced beef or pork.

Predictive Deviation (RPD). No test set was used for regression models due to the relatively low number of samples used to develop each model. In addition to obtaining a regression model for each adulterant, a general regression models was also developed where adulterants' ratios can be determined using the same model apart from prior information about the adulterant type. The model was developed using either all or selected features. In the latter case, only the common selected features between all classes were applied. MATLAB® was used for implementing image processing operations, and applying different machine learning algorithms in this study.

3. Results and discussion

3.1. First stage classification results (sample is pure or adulterated)

Classification results for the first stage (i.e., pure and adulterated) using different resampling techniques are shown in Table 2. In general, oversampling yielded better performance than downsampling. Oversampling by repetition resulted in similar classification accuracies for individual color channels. Classification accuracy values obtained by the SMOTE algorithm showed that combined features yielded results as high as 93.2%. Features obtained from gray-level, red, green, blue, and saturation had accuracy values of 92.9%, 88.0%, 91.0%, 89.9%, and 91.0%, respectively. In the case of downsampling, the classification accuracy for models obtained from all channels ranged from 87.0 to 88.1%. The classification accuracy results for color channels were 76.3–86.4%, 76.3–81.4%, 76.3–81.4%, 79.7–83.1%, 78.3–88.1% for gray-level, red, green, blue, and saturation, respectively. In the case of selected features, the minimum and maximum classification accuracy values for downsampling were 72.9, and 84.7%. While the classification accuracy results for oversampling and oversampling by SMOTE were 100% and 87.2%, respectively. Table 3 shows the confusion matrix for the classification models obtained after applying the SMOTE algorithm. The individual classification accuracies using all features were 82.7% for pure samples and 97.7% for adulterated samples. For selected features, the accuracy values were 74.5% for pure and 93.9% for adulterated samples. These results are comparable to those from other studies that used spectroscopic systems for meat adulteration detection [19,20]. The PCA score plot is shown in Fig. 5. The clusters for pure and adulterated samples are not separated, which is possibly a result of the presence of beef or pork in all adulterated and unadulterated samples. It is also noted that the PC scores for pure samples show more scattering than those for adulterated samples which is a result of the variability of the pure samples which had plant and animal origins, whereas, the

Table 2
Classification results for the test set for pure and adulterated meat samples (stage 1) using LDA, and all or selected features from different color channels along with different resampling techniques.

	Source of features	No. of features	Classification accuracies for the training-testing sets (%)			
			Downsampling		Oversampling (by repetition)	Oversampling (by SMOTE Algorithm)
			Minimum	Maximum		
All features	**All features**	**230**	86.4–87.0	90.6–88.1	99.3–98.9	94.7–93.2
	Gray-level	**46**	90.6–76.3	93.8–86.4	98.8–98.6	92.0–92.9
	Red	**46**	87.5–76.3	91.5–81.4	98.9–99.1	92.2–88.0
	Green	**46**	86.7–79.7	93.8–83.1	99.1–98.0	92.2–91.0
	Blue	**46**	89.7–78.3	93.8–88.1	99.1–98.4	92.2–89.9
	Saturation	**46**	82.4–81.0	90.0–83.1	98.0–98.4	92.8–91.0
Selected features		**8**	74.6–72.9	90.6–84.7	100–100	88.2–87.2

Table 3
Confusion matrices for the test set for pure vs. adulterated meat and plant proteins using LDA, and all or selected features based on the SMOTE oversampling algorithm.

			Pure	Adulterated
All features	**Predicted class**	**Pure**	91	6
		Adulterated	19	252
		Classification accuracy (%)	**82.7**	**97.7**
Selected features		**Pure**	80	17
		Adulterated	30	241
		Classification accuracy (%)	**74.5**	**93.9**
			Target (true) class	

adulterated samples contained mainly meats. The selected features for the first classification stage are displayed in Fig. 6. There were only 8 features selected for the first stage. Among the studied channels, the gray-level had 7 selected features in addition to only 1 feature selected from the green channel. While various color channels did not show a significant difference for classification performance, the selected features yielded slightly lower performance in the case of downsampling. Models obtained using selected features along with the oversampling technique yielded similar or better classification performance than those deduced using downsampling. This shows the redundant information contained in all features (236) compared with only 8 selected features which accounts for only 3.5% of the total number of features (see Fig. 6).

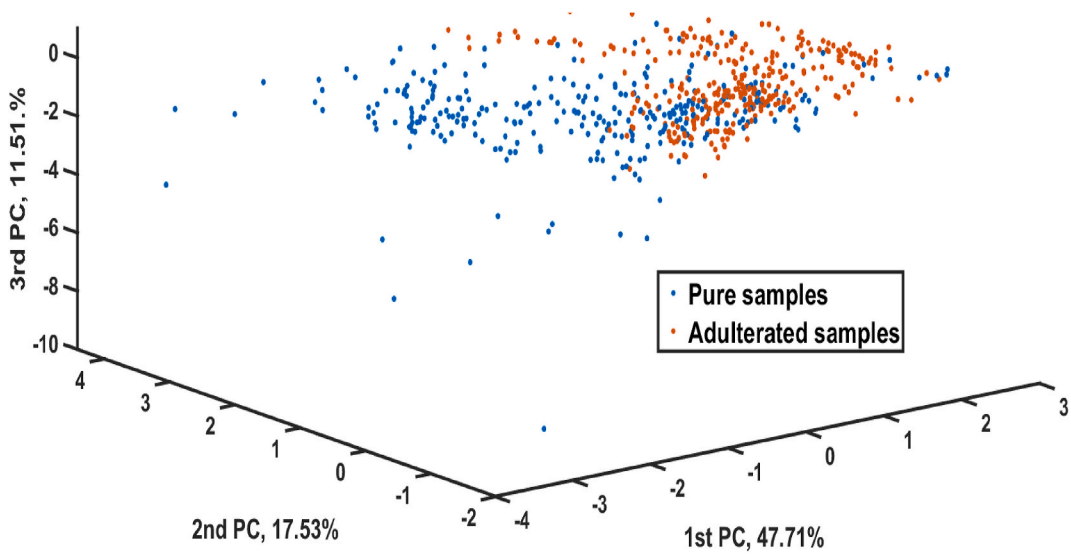

Fig. 5. PCA score plot for the first stage of classification of pure or adulterated samples using a downsampling technique, and the LDA classifier.

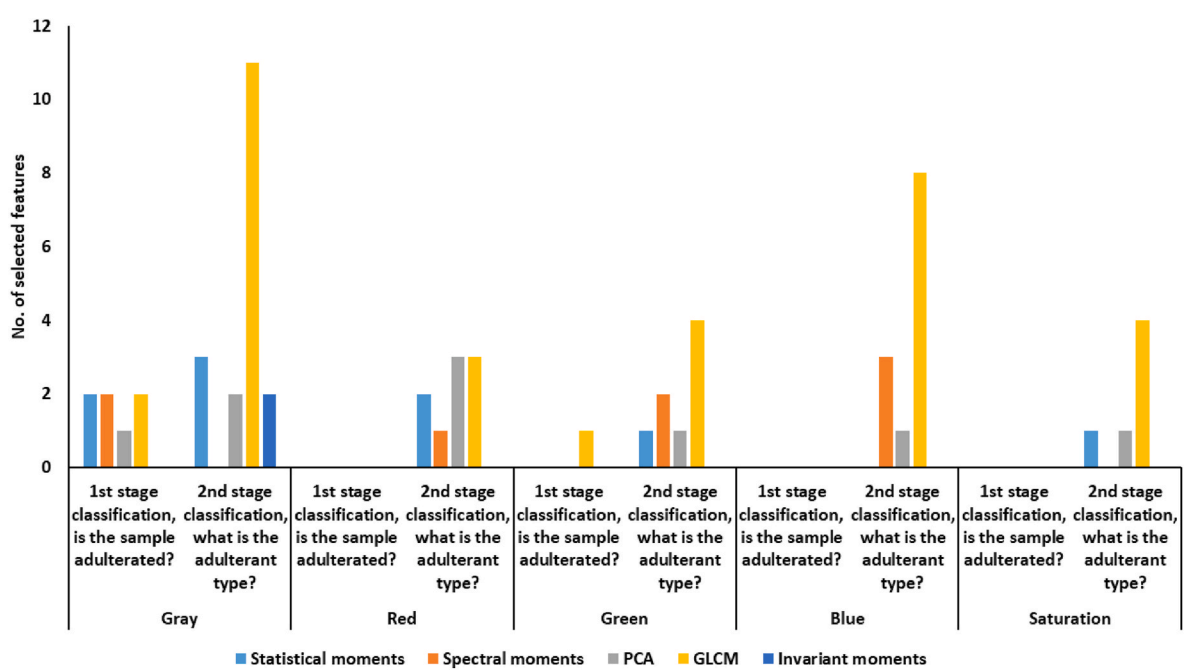

Fig. 6. Selected features for classifying pure vs. adulterated samples and adulterated samples using different features extracted from color coordinates, and the LDA classifier. (For interpretation of the references to color in this figure legend, the reader is referred to the Web version of this article.)

3.2. Second stage classification results (type of adulterant)

Table 4 shows classification accuracies for samples correctly classified as adulterated in the first stage. Models based on all features yielded classification accuracy as high as 76.1%, which is significantly higher than those deduced from other color channels, which ranged from 48.9% to 53.9%. For models developed using selected features, the classification accuracy was 63.8%. However, there were only 53 selected features compared with 230 total features, which still represents the efficacy of the sequential feature selection algorithm applied in this study. The confusion matrices shown in Table 5 demonstrate the effect of different adulterants on classification performance. In the case of all feature-models, beef adulterated with SP, chicken, or WG as well as pork adulterated with SP yielded relatively high accuracy, which ranged from 71.9 to 87.7%. Beef adulterated with pork yielded lower accuracy (65.8%), and beef adulterated with Pork + SP had the lowest accuracy (46.2%). The misclassification is mostly due to that the presence of beef or pork was obvious in all adulterated samples. This effect was higher in beef sample adulterated with Pork + SP as the total number of data points in the test set was much lower than other classes. It can also be observed from Fig. 1 that in the high ratios of SP in beef, SP in pork, or Pork + SP in beef, samples can be classified to the wrong class as the color and texture features are slightly similar [59]. Therefore, having a larger data set reduces the classification error as the training model will be more robust when it is developed with a repeated cross-validation, or bootstrap methodologies as they showed the advantages of producing less overfitting and more practical prediction errors [51]. In the case of models developed using selected features, only beef, and pork adulterated with SP achieved classification accuracies of 71.9% and 89.7%, respectively. Beef adulterated with pork, chicken, WG, or SP + Pork achieved classification accuracy values of 41.0%, 64.9%, 50.9%, and 45.5%, respectively. Selected features for classifying adulterated samples, as shown in Fig. 6, were considerably more than those needed for classifying samples into pure or adulterated. This increase was expected as the adulterated samples had foreign components compared with pure samples, and the classifier was required to get trained then to identify the adulterant's origin, not just to evaluate the presence of adulterants or not. It is also important to note that while there were mostly no features needed from color channels to differentiate between pure and adulterated samples, identifying the adulterant type required more information from various color channels utilized in this study. Furthermore, the gray-level was more effective than other color coordinates and had 18 selected features for the stage two classification models. Whereas the blue, red, green, and saturation channels contributed to 12, 9, 8, and 6 selected features, respectively. It is worth stating that gray-level images are more common in image processing and pattern classification when monochromatic-based vision systems are utilized [43]. GLCM yielded 30 selected features compared with 7, 6, 8, and 2 features selected based on statistical moments, spectral moments, PCA, and invariant moments. Texture features obtained from the GLCM were, therefore, more critical for identifying foreign materials added to beef or pork samples. The advantage of GLCM is that it incorporates the spatial and intensity levels between neighboring pixels in the image which indeed helps identify foreign materials (i.e. adulterants) in the sample [55]. The importance of GLCM features was confirmed by previous studies that applied GLCM-based features for potatoes [60], beef tenderness [61,62], classification of bovine meat based on muscle type, age, and breed [63].

While most color-based imaging for meat quality assessment available in the literature targeted the evaluation of freshness and color, the previous studies that focused on meat adulteration utilized spectroscopic techniques such as NIR, and Fourier-Transform Infrared (FTIR) spectroscopy, or hyperspectral imaging. The previous work demonstrated that hyperspectral imaging could achieve classification accuracies of 100% for classifying unadulterated and adulterated bovine cut muscles or minced meat adulterated with animal and plant proteins [20]. ultraviolet (UV), Vis, NIR, and/or mid-infrared (MIR) were also successfully applied with classification accuracies of 69–100% to detect minced beef or lamb adulterated with pork, chicken, and horsemeat [64], minced beef adulterated with turkey [17], raw and cooked beef patties adulterated with pork, skimmed milk or mutton [65], minced beef and pork adulterated with animal and plant proteins [19]. Multispectral imaging was also demonstrated as a successful technique to identify minced beef adulterated with horsemeat [66] or pork [15] with classification accuracy as high as 98.48%. FTIR (4000-700 cm^{-1}) was tested to assess the presence of pork in beef jerky with classification accuracies as high as 100% [67]. While the aforementioned studies demonstrate the capabilities of optical techniques for detecting adulteration in meat, the majority utilized large and expensive systems which differ from the small and low-cost color imaging system used in this current work.

Table 4
Classification results obtained for adulterated meat samples (stage 2) using LDA, and all or selected features from different color channels under several methods for imbalanced classes.

	No. of samples	Source of features	Classification accuracy (%)	
			Training set	Testing set
All features	**230**	**All channels**	80.00	76.1
	46	**Gray-level**	57.6	53.9
	46	**Red**	54.5	53.9
	46	**Green**	57.9	55.7
	46	**Blue**	57.2	50.4
	46	**Saturation**	55.5	48.9
Selected features	**53**		70.7	63.8

3.3. Stage three regression results (quantification of adulterant)

Regression Tree (RT) model results for quantifying the adulterant level in each adulterated sample using all or selected features are shown in Table 6. Using all features, the prediction of pork quantity in minced beef samples had the highest r(RPD) values of 98.0%(5.0%). In the case of beef adulterated with SP, chicken, WG, and Pork + SP, the r(RPD) values were 97.7%(4.7%), 96.2%(3.7%), 97.5%(4.3%), and 87.0% (2.1%), respectively. For pork adulterated with SP, the r(RPD) values were 97.8%(4.8%). Regression models using selected features achieved lower performance compared to those reported using all features. Regression models for beef adulterated with pork, SP, chicken, WG, and SP + Pork yielded r(RPD) values of 92.4%(2.6), 86.4%(2.0), 94.5%(3.2), 91.3%(2.5), and 80.8%(1.7), respectively; while those for pork adulterated with SP were 89.2%(2.2). There were 105 common selected features for regression and the general regression models based on all and the common selected features had r(RPD) values of 92.6%(2.7%) and 92.5%(2.7%), respectively. Regression models yielded relatively high RMSEcv values compared with the lowest adulteration ratio (1%) and this could be decreased further by testing a larger number of samples, which would reduce training errors [56]. Current results indicate that using all features for predicting the adulteration level was the best method as the models had lower errors. Similar to the classification results, the GLCM features represented the majority of selected features used to develop the regression models which proves that such features hold the most influencing information about the adulterants [68]. The features needed to explain the exact quantity of adulterant in each mixture, as shown in Fig. 7, are more than those needed to differentiate between pure or adulterated samples. This can be explained by the similarity between different classes that include beef, SP, or pork. Thus, extracted features, especially from images with low adulterant concentrations, can lead to misclassification between the different classes. Results indicated that there were 71 selected GLCM features, whereas

Table 5
Confusion matrices for the test set obtained adulterated meat samples (stage 2) using LDA, and all or selected features.

			Beef+ Pork	Beef + SP	Beef+ Chicken	Beef + WG	Pork + SP	Beef+ Pork + SP
All features	**Predicted class**	Beef + Pork	25	6	7	0	0	0
		Beef + SP	3	41	2	1	2	1
		Beef + Chicken	10	5	44	9	1	1
		Beef + WG	0	5	4	47	1	0
		Pork + SP	0	0	0	0	50	5
		Beef + Pork + SP	0	0	0	1	3	6
		Classification accuracy (%)	**65.8**	**71.9**	**77.2**	**81.0**	**87.7**	**46.2**
Selected features	**Predicted class**	Beef + Pork	16	4	8	9	2	0
		Beef + SP	11	41	7	3	1	0
		Beef + Chicken	7	2	37	13	0	1
		Beef + WG	3	9	4	29	2	2
		Pork + SP	2	1	1	2	52	9
		Beef + Pork + SP	0	0	0	1	1	10
		Classification accuracy (%)	**41.0**	**71.9**	**64.9**	**50.9**	**89.7**	**45.5**
		Target (true) class						

Table 6
Regression results using RT and cross-validation for quantifying adulterant level using all or selected features along with regression trees.

	Adulterated (adulterant)	r (%)	$RMSE_{CV}$ (%)	RPD
All features	Beef (Pork)	98.0	3.3	5.0
	Beef (SP)	97.7	2.6	4.7
	Beef (Chicken)	96.2	3.3	3.7
	Beef (Wheat Gluten)	97.5	2.8	4.3
	Pork (SP)	97.8	2.5	4.8
	Beef (Pork + SP)	87.0	6.0	2.1
	General model	92.6	4.9	2.7
Selected features	Beef (Pork)	92.4	6.5	2.6
	Beef (SP)	86.4	6.1	2.0
	Beef (Chicken)	94.5	3.8	3.2
	Beef (Wheat Gluten)	91.3	4.9	2.5
	Pork (SP)	89.2	5.4	2.2
	Beef (Pork + SP)	80.8	7.3	1.7
	General model	92.5	4.9	2.7

the selected features from statistical moments were 13. The number of features selected from spectral moments, PCA, and invariant moments was 21, 29, and 32. The Considering the color channels, the number of features selected from gray-level, red, green, blue, and saturation were 24, 34, 36, 40, and 32, respectively. The results in this study are distinguishable compared with similar studies due to the simplicity of the RGB system and the large range of adulterants, and the different ratios of adulteration studied. Weng, Guo [69] used Vis/NIR spectroscopy (350–2500 nm) to detect 4 pork ratios (4%, 12%, 20%, and 30%, w/w) in minced beef, and the developed models were able to achieve a maximum R^2 value of 97.3%. In a study conducted by Zhao, Feng [70], a hyperspectral imaging system (400–1000 nm) was used to quantify different ratios of spoiled beef in minced beef, and the R^2 and RMSE values of the developed regression models were 94% and 5.39%, respectively. Spoiled beef adulterating minced beef was also studied using UV/Vis/NIR (200–1100 nm), and the R^2 (RMSE) values of the developed models were 91% and 2.68% [70]. A hyperspectral imaging system (400–1000 nm) was utilized to assess minced beef adulterated with different ratios of chicken, and the developed models had R^2 value

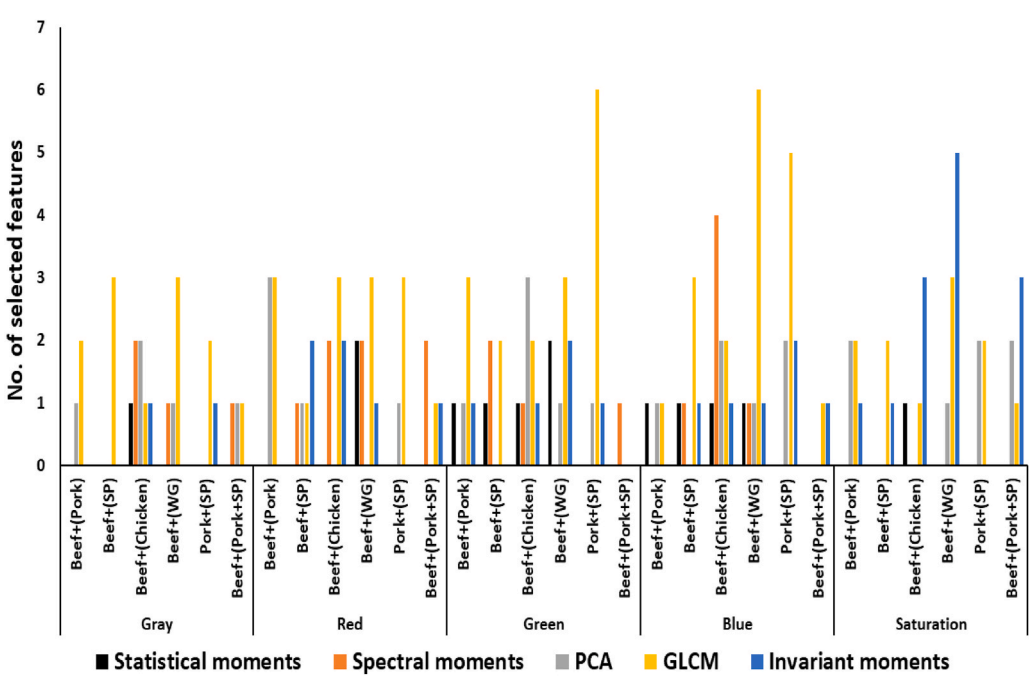

Fig. 7. Selected features from color coordinates for quantifying the plant and animal adulterants ratios in minced beef or pork using RT. (For interpretation of the references to color in this figure legend, the reader is referred to the Web version of this article.)

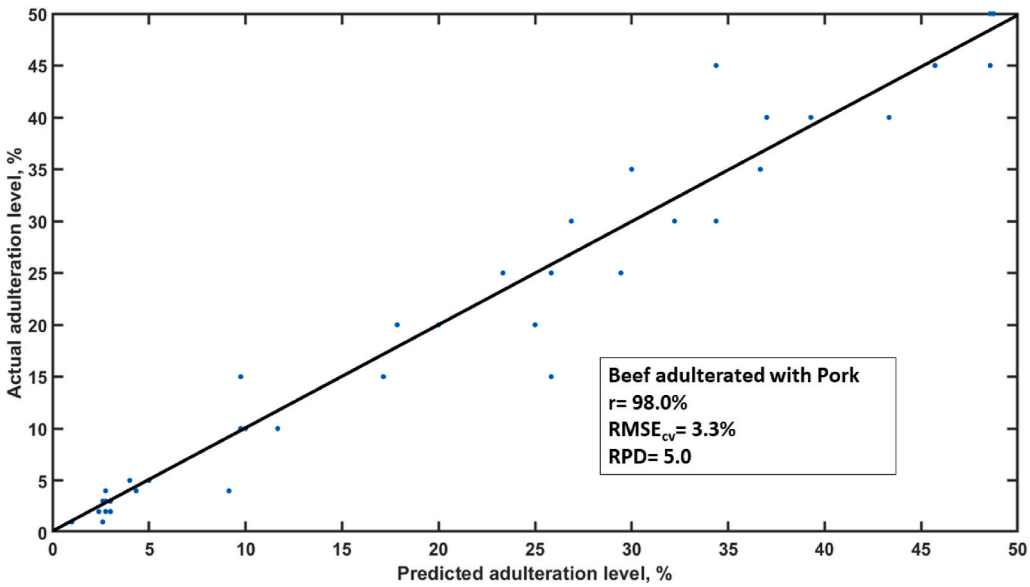

Fig. 8. Scatter plot for actual and predicted adulteration ratios for beef adulterated with soybean protein (SP) based on RT models using all features from an RGB color system. (For interpretation of the references to color in this figure legend, the reader is referred to the Web version of this article.)

as high as 97% [71]. While some of the previous studies presented the feasibility of applying optical sensors to evaluate the ratios of various adulterants in meats, this study presents a cost-effective technology and data analysis methodology that suits small meat processing businesses that want to assure the quality and legality of their products. The system can also be embedded in a cloud-based IoT scheme that can provide assurance to a variety of stakeholders across the supply chain including regulatory agencies. Fig. 8 shows an example of the scatter graphs for regression models that show the relationship between predicted and actual adulteration ratios for Beef + SP. While most predicted adulterant's values were lower than the actual values, the majority of error values were uniformly distributed demonstrating that the model performance does not reduce at different adulteration ratios.

4. Conclusions

The current study demonstrates the potential of a cost-effective and easy to use technology for the detection and quantification of different adulterants in minced beef and pork. This technology could be used across the meat supply chain for enhanced traceability. Plant and animal-based proteins were assessed as adulterants for minced beef or pork. Although the plant proteins used in manufacturing beef patties are usually in powder form, this study provides a dependable methodology that can build upon for obtaining quick evaluation of minced meats. This study presented a complex scenario with a range of different adulteration ratios up to 50%. Results of extracted features showed the importance of using gray-level images in differentiating between pure and adulterated samples where all samples were correctly classified. Beef, chicken, and wheat gluten adulterants were easier to identify than pork or soybean protein. Identifying adulterant type was promising with an individual accuracy of 46.2–87.7% when using all features and 41.0–89.7% when using selected features (primarily from GLCM). Quantifying the ratios of each adulterant was possible, and the r value reached 87.0–98.0% and 80.8–94.5% using all and selected features, respectively. While the system presented in this study cannot be used to detect sub-surface adulterants in minced meat, and it will be more difficult to identify plant proteins in the powder form, it can still serve as a fast, low-cost, and effective method for accurate, and initial decision making for meat adulteration in the food industry, or government agencies. Moreover, the system can be fused with other optical sensors such as spectroscopic or multispectral imaging to attain more comprehensive quality evaluation of possible adulteration. To boost the performance of the system, diversity in meat sources, breeds, muscles, powder plant proteins, and storage conditions should be considered in future work. Moreover, the performance of the machine learning models could be improved by training larger data set of images to optimize the models using more advanced machine learning methodologies such as deep learning.

Declaration of competing interest

None.

Acknowledgements

The information reported in this paper is a project of the Kentucky Agricultural Experiment Station and it is published with the approval of the Director. This work was supported by the National Institute of Food and Agriculture, U.S. Department of Agriculture, Hatch- Multistate project #: 1007893.

References

[1] FAO, Livestock primary [cited 2020 22/1/2020]; Available from, http://www.fao.org/faostat/en/#data/QL, 2020.
[2] NAMI, The United States meat industry at a glance [cited 2020 22/1/2022]; Available from: https://www.meatinstitute.org/index.php?ht=d/sp/i/47465/pid/47465, 2020.
[3] J. Spink, D.C. Moyer, Defining the public health threat of food fraud, J. Food Sci. 76 (9) (2011) R157–R163.
[4] N.O. Madichie, The European'horsemeat scandal': a welcome opportunity for the halal supply chain? J. Cust. Behav. 14 (1) (2015) 63–82.
[5] R.G. Kauffman, Meat composition, Meat science and applications 1 (2001) 1–127.
[6] F. Toldrá, Handbook of Meat Processing, John Wiley & Sons, 2010.
[7] G. Heinz, P. Hautzinger, Meat Processing Technology for Small to Medium Scale Producers, 2007.
[8] A. Germini, A. Tonelli, Detection of genetically modified organisms in processed meats and poultry, in: L.M. Nollet, F. Toldrá (Eds.), Handbook of Processed Meats and Poultry Analysis, CRC Press, 2009, pp. 545–570.
[9] M.C.G. López, M.L.M. Alegre, in: L.M.L. Nollet, F. Toldra (Eds.), Detection of Adulterations: Addition of Foreign Proteins. Safety Analysis of Foods of Animal Origin, CRC Press, Boca Raton, 2011, pp. 155–185.
[10] A. Frouin, C. Barraud, D. Jondeau, Detection des Proteines de Soja ou de Lait dans les Produits de Viande Sterilises ou Non, Ann. Fals. Exp. Chim 66 (1973) 214.
[11] H. Brehmer, S. Schleicher, U. Borowski, Determination of Soya Protein, Pea Protein and Gluten in Frankfurter-type Sausages by Means of an Enzyme-Linked-Immunosorbent-Assay (ELISA), 1999. Fleischwirtschaft (Germany).

[12] M. Criado, et al., Detection and quantitation of additions of soybean proteins in cured-meat products by perfusion reversed-phase high-performance liquid chromatography, J. Separ. Sci. 28 (9-10) (2005) 987–995.
[13] D. Maede, A strategy for molecular species detection in meat and meat products by PCR-RFLP and DNA sequencing using mitochondrial and chromosomal genetic sequences, Eur. Food Res. Technol. 224 (2) (2006) 209–217.
[14] M. Kamruzzaman, et al., Assessment of visible near-infrared hyperspectral imaging as a tool for detection of horsemeat adulteration in minced beef, Food Bioprocess Technol. 8 (5) (2015) 1054–1062.
[15] A. Ropodi, et al., Multispectral image analysis approach to detect adulteration of beef and pork in raw meats, Food Res. Int. 67 (2015) 12–18.
[16] M. Al-Sarayreh, et al., Detection of red-meat adulteration by deep spectral–spatial features inJ. Imag. hyperspectral images, J. Imaging 4 (5) (2018) 63.
[17] C. Alamprese, et al., Detection of minced beef adulteration with Turkey meat by UV–vis, NIR and MIR spectroscopy, LWT-Food Sci. Technol. 53 (1) (2013) 225–232.
[18] N. Morsy, D.-W. Sun, Robust linear and non-linear models of NIR spectroscopy for detection and quantification of adulterants in fresh and frozen-thawed minced beef, Meat Sci. 93 (2) (2013) 292–302.
[19] A. Rady, A. Adedeji, Assessing different processed meats for adulterants using visible-near-infrared spectroscopy, Meat Sci. 136 (2018) 59–67.
[20] A. Rady, A.A. Adedeji, Application of hyperspectral imaging and machine learning methods to detect and quantify adulterants in minced meats, Food Anal. Methods (2020) 1–12.
[21] D. Santos Jr., et al., Laser-induced breakdown spectroscopy for analysis of plant materials: a review, Spectrochim. Acta B Atom Spectrosc. 71 (2012) 3–13.
[22] X. Zou, J. Zhao, Nondestructive Measurement in Food and Agro-Products, Springer, 2015.
[23] K. Chen, et al., Color grading of beef fat by using computer vision and support vector machine, Comput. Electron. Agric. 70 (1) (2010) 27–32.
[24] X. Sun, et al., A digital image method for measuring and analyzing color characteristics of various color scores of beef, in: 2009 2nd International Congress on Image and Signal Processing, IEEE, 2009.
[25] D. Gerrard, X. Gao, J. Tan, Beef marbling and color score determination by image processing, J. Food Sci. 61 (1) (1996) 145–148.
[26] X. Meng, et al., Evaluation of beef marbling grade based on advanced watershed algorithm and neural network, Adv. J. Food Sci. Technol. 6 (2) (2014) 206–211.
[27] T. McDonald, Y. Chen, Visual characterization of marbling in beef ribeyes and its relationship to taste parameters, Transactions of the ASAE 34 (6) (1990) 2499–2504.
[28] C.-J. Du, et al., Development of a hybrid image processing algorithm for automatic evaluation of intramuscular fat content in beef M. longissimus dorsi, Meat Sci. 80 (4) (2008) 1231–1237.
[29] H. Hwang, et al., Hybrid image processing for robust extraction of lean tissue on beef cut surfaces, Comput. Electron. Agric. 17 (3) (1997) 281–294.
[30] P. Jackman, D.-W. Sun, P. Allen, Prediction of beef palatability from colour, marbling and surface texture features of longissimus dorsi, J. Food Eng. 96 (1) (2010) 151–165.
[31] M. O'sullivan, et al., Evaluation of pork colour: prediction of visual sensory quality of meat from instrumental and computer vision methods of colour analysis, Meat Sci. 65 (2) (2003) 909–918.
[32] J. Lu, et al., Evaluation of pork color by using computer vision, Meat Sci. 56 (1) (2000) 57–60.
[33] F. Tan, et al., Assessment of fresh pork color with color machine vision, J. Anim. Sci. 78 (12) (2000) 3078–3085.
[34] M. Chmiel, et al., Use of computer vision system (CVS) for detection of PSE pork meat obtained from m. semimembranosus, LWT-Food Sci. Technol. 65 (2016) 532–536.
[35] M. Chmiel, M. Słowiński, K. Dasiewicz, Lightness of the color measured by computer image analysis as a factor for assessing the quality of pork meat, Meat Sci. 88 (3) (2011) 566–570.
[36] X. Sun, et al., Prediction of pork color attributes using computer vision system, Meat Sci. 113 (2016) 62–64.
[37] K. Xiao, G. Gao, L. Shou, An improved method of detecting pork freshness based on computer vision in on-line system, Sensors & Transducers 169 (4) (2014) 42.
[38] J.-H. Liu, et al., Predicting pork loin intramuscular fat using computer vision system, Meat Sci. 143 (2018) 18–23.
[39] A. Taheri-Garavand, et al., Meat Quality Evaluation Based on Computer Vision Technique: A Review, Meat science, 2019.
[40] J.J. Neto, J.A.d. Santos, W.R. Schwartz, Meat Adulteration Detection through Digital Image Analysis of Histological Cuts Using LBP, 2016 arXiv preprint arXiv: 1611.02260.
[41] R.C. Gonzalez, R.E. Woods, B.R. Masters, Digital Image Processing, third ed., Pearson International Edition, 2008.
[42] W.K. Pratt, Image Enhancement, Digital image processing, 2001, pp. 247–307.
[43] B. Jahne, Practical Handbook on Image Processing for Scientific and Technical Applications, CRC press, 2004.
[44] H. Zhou, J. Wu, J. Zhang, Digital Image Processing: Part II, Bookboon, 2010.
[45] C. Palm, Color texture classification by integrative co-occurrence matrices, Pattern Recogn. 37 (5) (2004) 965–976.
[46] R.C. Gonzalez, R.E. Woods, S.T. Eddins, Digital Image Procesisng Using Matlab, Gatesmark Publishing, USA, 2009.
[47] R.M. Haralick, K. Shanmugam, I. Dinstein, Textural features for image classification, IEEE Transactions on Systems, Man, and Cybernetics 3 (6) (1973) 610–621. SMC.
[48] F. Albregtsen, Statistical Texture Measures Computed from Gray Level Coocurrence Matrices, vol. 5, Image processing laboratory, department of informatics, university of oslo, 2008, 5.
[49] J.-B. Martens, L. Meesters, Image dissimilarity, Signal Process. 70 (3) (1998) 155–176.
[50] D.A. Clausi, An analysis of co-occurrence texture statistics as a function of grey level quantization, Can. J. Rem. Sens. 28 (1) (2002) 45–62.
[51] K. Varmuza, P. Filzmoser, Introduction to Multivariate Statistical Analysis in Chemometrics, CRC press, 2016.
[52] Y. Sun, A.K. Wong, M.S. Kamel, Classification of imbalanced data: a review, Int. J. Pattern Recogn. Artif. Intell. 23 (2009) 687–719, 04.
[53] N.V. Chawla, et al., SMOTE: synthetic minority over-sampling technique, J. Artif. Intell. Res. 16 (2002) 321–357.
[54] H. Han, W.-Y. Wang, B.-H. Mao Borderline-SMOTE, A new over-sampling method in imbalanced data sets learning, in: International Conference on Intelligent Computing, Springer, 2005.
[55] S. Theodoridis, K. Koutroumbas, Pattern Recognition, Academic Press, Elsevier, 2003.
[56] R.O. Duda, P.E. Hart, D.G. Stork, Linear discriminant function, in: Pattern Classification, John Wiley & Sons, Inc., NY, USA, 2012, pp. 215–281.
[57] L. Rokach, Pattern Classification Using Ensemble Methods, vol. 75, World Scientific, 2010.
[58] C.M. Bishop, Linear models for classification, in: Pattern Recognition and Machine Learning, Springer, 2006, pp. 179–224.
[59] R. Mancini, M. Hunt, Current research in meat color, Meat Sci. 71 (1) (2005) 100–121.
[60] F. Mendoza, P. Dejmek, J.M. Aguilera, Colour and image texture analysis in classification of commercial potato chips, Food Res. Int. 40 (9) (2007) 1146–1154.
[61] J. Li, et al., Image texture features as indicators of beef tenderness, Meat Sci. 53 (1) (1999) 17–22.
[62] X. Sun, et al., Predicting beef tenderness using color and multispectral image texture features, Meat Sci. 92 (4) (2012) 386–393.
[63] O. Basset, et al., Application of texture image analysis for the classification of bovine meat, Food Chem. 69 (4) (2000) 437–445.
[64] A. López-Maestresalas, et al., Detection of minced lamb and beef fraud using NIR spectroscopy, Food Control 98 (2019) 465–473.
[65] H. Ding, R. Xu, Near-infrared spectroscopic technique for detection of beef hamburger adulteration, J. Agric. Food Chem. 48 (6) (2000) 2193–2198.
[66] A.I. Ropodi, E.Z. Panagou, G.-J.E. Nychas, Multispectral imaging (MSI): a promising method for the detection of minced beef adulteration with horsemeat, Food Control 73 (2017) 57–63.
[67] B. Kuswandi, et al., Application of class-modelling techniques to infrared spectra for analysis of pork adulteration in beef jerkys, J. Food Sci. Technol. 52 (12) (2015) 7655–7668.
[68] C. Zheng, D.-W. Sun, L. Zheng, Recent applications of image texture for evaluation of food qualities—a review, Trends Food Sci. Technol. 17 (3) (2006) 113–128.
[69] S. Weng, et al., Rapid detection of adulteration of minced beef using Vis/NIR reflectance spectroscopy with multivariate methods, Spectrochim. Acta Mol. Biomol. Spectrosc. 230 (2020) 118005.
[70] H.-T. Zhao, et al., Application of invasive weed optimization and least square support vector machine for prediction of beef adulteration with spoiled beef based on visible near-infrared (Vis-NIR) hyperspectral imaging, Meat Sci. 151 (2019) 75–81.
[71] M. Kamruzzaman, Y. Makino, S. Oshita, Rapid and non-destructive detection of chicken adulteration in minced beef using visible near-infrared hyperspectral imaging and machine learning, J. Food Eng. 170 (2016) 8–15.